# Experimental Identification of the Yaw Damping Derivative of a Flapping-Wing Micro Air Vehicle

D.-J. Liu and W.-L. Chan*
National Cheng Kung University, No. 1, Ta-Hsueh Road, Tainan, Taiwan

http://www.imavs.org/

ABSTRACT

This paper presents an experimental method for identifying the yaw damping derivative of a tailed flapping-wing micro air vehicle (FWMAV). Although flapping-wing vehicles exhibit highly coupled unsteady aerodynamics, experimental characterization of their lateral–directional stability derivatives remains limited. A robotic-arm-based test platform was developed to impose controlled yaw motions under prescribed angles of attack and sideslip conditions while measuring the resulting aerodynamic forces and moments. The platform integrates a six-axis force/torque sensor, optical motion capture, synchronized data acquisition, and a fan-array facility to reproduce a forward-flight inflow condition.

Experimental results show that the yawing moment exhibits a clear and repeatable dependence on yaw rate, enabling identification of the yaw damping derivative, $N_r$. The identified values remain negative throughout the tested conditions, indicating that the vehicle generates a restoring yawing moment opposing yaw-rate perturbations. In contrast, the side-force response shows no consistent yaw-rate dependence, while the roll moment is governed primarily by sideslip angle rather than yaw rate. These findings provide experimental evidence of passive yaw damping in a tailed FWMAV and demonstrate the feasibility of robotic-arm-based forced-motion testing for identifying lateral–directional stability derivatives to support flight dynamics modeling and controller development.

## 1 INTRODUCTION

Flapping-wing micro air vehicles (FWMAVs) represent a class of bio-inspired flying machines that generate lift and thrust through reciprocating wing motion. At small scales and low Reynolds numbers, their aerodynamic behavior differs substantially from that of conventional fixed-wing and rotary-wing vehicles. Unsteady mechanisms such as clap-and-fling, leading-edge vortex formation, wake capture, and wing flexibility contribute significantly to their force and moment generation [1, 2, 3, 4]. These mechanisms offer potential advantages in agility and low-speed flight, but they also make the dynamic modeling and control of FWMAVs challenging.

For control-oriented flight dynamics, aerodynamic stability derivatives provide a compact way to describe how forces and moments vary with motion states such as angle of attack, sideslip angle, and angular rates. However, compared with conventional aircraft, the stability derivatives of FWMAVs remain insufficiently characterized. Existing studies have examined insect flight stability, simulation-based FWMAV dynamics, and system identification of flapping-wing vehicles [5, 6, 7, 8]. Among experimental FWMAV studies, the DelFly family is one of the few platforms for which dynamic models have been identified from flight data [9, 10]. Such free-flight identification is valuable because it directly reflects the behavior of the vehicle in flight, but it is naturally limited to flight regimes that are stable, repeatable, and safely achievable.

A complementary approach is to prescribe controlled motion in a laboratory environment while measuring the resulting aerodynamic forces and moments. This idea is closely related to the classical forced-oscillation method used for aircraft stability-derivative identification, in which a model is driven about a specified axis and the aerodynamic response is measured [11]. Robotic-arm-based aerodynamic testing extends this idea by allowing flexible motion trajectories and large attitude excursions. In previous work, a fan-array robotic-arm method was developed for CKopter-1 and used to identify pitch-rate stability derivatives over a broad angle-of-attack range [12]. That study demonstrated that the method can provide useful dynamic-derivative data even in regimes where sustained free flight is not feasible. The present work extends this methodology from longitudinal pitch-rate dynamics to lateral–directional yaw-rate excitation.

In lateral–directional dynamics, yaw damping is a key indicator of directional stability. The yaw-moment derivative with respect to yaw rate, $N_r$, describes how the yawing moment changes in response to yaw-rate perturbations. A negative $N_r$ indicates that the vehicle generates a yawing moment opposing the yawing motion, thereby providing stabilizing yaw damping. Such damping is particularly important for FWMAVs because their low inertia, unsteady aerodynamics, and multi-axis coupling can make the lateral–directional response difficult to predict from geometry alone. Passive

*Email address: woeileong_chan@gs.ncku.edu.tw

aerodynamic damping has also been discussed in the context of flapping flight and biological flyers, where it contributes to disturbance rejection and flight stability [13, 14].

This paper presents a robotic-arm-based experimental investigation of the yaw damping characteristics of a tailed flapping-wing micro air vehicle (FWMAV). Controlled yaw-sweep motions are imposed under prescribed angles of attack and sideslip conditions while synchronized force/moment and motion measurements are acquired. The primary objective is to experimentally identify the yaw damping derivative, $N_r$, and to characterize the associated lateral-directional aerodynamic responses. The proposed methodology extends forced-motion testing to flapping-wing MAVs and provides an experimental framework for identifying lateral-directional stability derivatives to support flight dynamics modeling and controller development.

## 2 Experimental Setup and Methodology

### 2.1 Flapping-wing MAV platform

The test vehicle used in this study is the tailed flapping-wing micro air vehicle (CKopter-1) previously reported by Chan *et al.* [12]. The vehicle has a total mass of 17.25 g, a wingspan of 200 mm, and employs a pair of reciprocating wings to generate lift and thrust, while a conventional tail provides longitudinal and directional stability and control. A detailed description of the vehicle design, flapping mechanism, structural configuration, and aerodynamic characteristics can be found in [12].

The center of gravity (CG) of the fully assembled FWMAV was determined experimentally by balancing the vehicle on a fine support point until static equilibrium was achieved. The measured CG location was subsequently used to transform the forces and moments measured by the six-axis force sensor from the sensor reference frame to the vehicle CG. A detailed description of the coordinate transformation is available in [12].

To facilitate comparison with the previously identified longitudinal dynamic derivatives, the same experimental configuration and trim condition were adopted throughout this study. The flapping mechanism was operated at the experimentally determined steady-level-flight condition reported in [12], corresponding to a flapping frequency of 14 Hz under a nominal incoming flow of approximately $2\ \mathrm{m/s}$. The elevator and rudder were fixed at their trim positions throughout all experiments so that variations in the measured aerodynamic forces and moments could be attributed primarily to the prescribed yaw motion.

The objective of the present experiments was to identify the yaw damping derivative, $N_r$, under different angles of attack and sideslip conditions. In addition to the yawing moment, the side force and rolling moment were also examined to assess whether other lateral–directional aerodynamic derivatives associated with yaw-rate excitation could be reliably identified using the proposed robotic-arm-based experimental method.

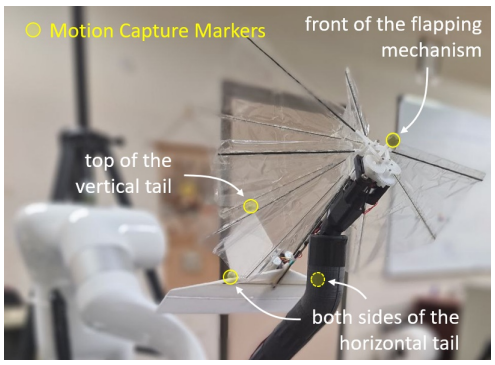


Figure 1: Tailed flapping-wing MAV platform used in this study.

### 2.2 Robotic-arm-based dynamic test setup

A robotic-arm-based experimental setup was developed to impose repeatable yaw motions on the FWMAV. The vehicle was mounted on a support structure connected to a six-axis force/torque sensor (ATI Nano17 Titanium, ATI Industrial Automation, USA), which measured the three-axis forces and moments throughout the prescribed yaw-sweep motion. The sensor outputs were synchronized with the robotic-arm motion and the optical motion-capture measurements for subsequent aerodynamic derivative identification. This setup extends the fan-array robotic-arm methodology previously developed for pitch-rate dynamic characterization of a flapping-wing MAV to the identification of lateral–directional derivatives under yaw-rate excitation [12].

An optical motion-capture system (Vicon Motion Systems Ltd., UK) was used to measure the actual position and attitude of the FWMAV throughout each experiment. Although the robotic arm prescribed the desired yaw-sweep motion, the commanded trajectory was not used directly for aerodynamic derivative identification. Instead, the motion-capture measurements were used to determine the actual vehicle attitude and yaw rate, thereby accounting for any deviations arising from robot tracking errors, structural compliance, or mounting flexibility. The motion-capture and force/moment measurements were synchronized through a common frame-based data acquisition procedure, enabling the measured aerodynamic loads to be correlated with the instantaneous vehicle motion.

A fan-array flow facility was placed upstream of the model to generate a controlled incoming flow. Since the model was fixed to the robotic-arm platform, the incoming flow was used to reproduce the relative flow condition experienced during forward flight. The incoming flow velocity at the test location was measured using an Extech HD350 differential pressure manometer equipped with a Pitot tube. During fan-array operation, the measured velocity fluctuated about a

http://www.imavs.org/

http://www.imavs.org/

mean value of approximately 2 $\mathrm{m/s}$. Accordingly, all experiments were conducted under a nominal incoming flow condition of approximately 2 $\mathrm{m/s}$. A detailed characterization of the spatial velocity distribution and turbulence intensity of the fan-array flow was beyond the scope of the present study.

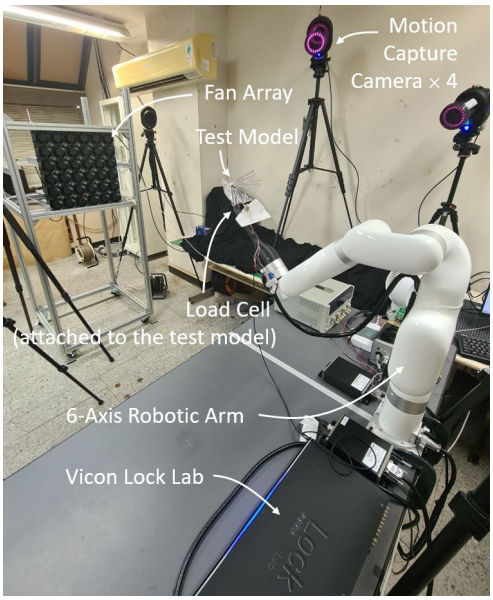


Figure 2: Synchronized robotic-arm-based experimental setup for yaw-rate derivative identification.

### 2.3 *Test conditions*

The experiments were conducted over a range of angles of attack and sideslip angles. The angle of attack was varied from 30° to 60°, encompassing the experimentally determined steady-level-flight trim condition of approximately 45° reported in [12]. This range was selected to characterize the yaw damping behavior in the vicinity of the nominal operating condition while also examining the influence of moderate deviations in angle of attack. The sideslip angle was varied within the prescribed yaw-sweep range.

For each angle-of-attack condition, the robotic arm executed a programmed yaw sweep from $\beta = -45°$ to $\beta = 45°$ at one of five prescribed sweep speeds, producing five corresponding yaw-rate conditions. To avoid the acceleration and deceleration phases associated with the reversal of the robotic-arm motion, only the data acquired between $\beta = -30°$ and $\beta = 0°$ were used for the subsequent analysis. This portion of the trajectory corresponded to the constant-angular-rate region, ensuring that the identified aerodynamic responses were associated with a well-defined yaw-rate excitation. Each test condition was repeated five times to evaluate experimental repeatability.

The lowest yaw-sweep speed was treated as the quasi-static reference condition, while the higher sweep speeds were used as the dynamic cases. By comparing the measured aerodynamic force and moment responses under different yaw-rate conditions, the yaw damping derivative was identified.

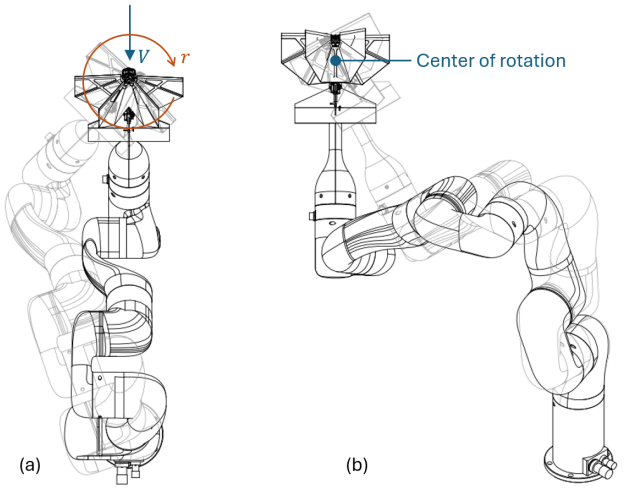


Figure 3: Robotic-arm yaw-sweep motion used to impose controlled sideslip and yaw-rate perturbations: (a) top view showing the incoming flow direction and yaw rate; (b) isometric view showing the center of rotation. The robotic arm executes a programmed yaw sweep from $\beta = -45°$ to $45°$. Only the constant-angular-rate segment between $\beta = -30°$ and $0°$ is included in the data analysis to avoid the acceleration and deceleration phases of the robotic-arm motion.

### 2.4 *Data processing*

The force/moment and motion-capture data were first synchronized using their corresponding frame indices. The force and moment signals were transformed from the sensor reference frame to the vehicle center of gravity using the experimentally determined CG location, filtered, and resampled to match the motion-capture sampling rate. Bias data collected without incoming flow and without flapping motion were subtracted to remove the static contribution of the mounting structure and sensor offsets.

The sideslip angle, $\beta$, was obtained from the attitude measured by the motion-capture system, while the yaw rate, $r$, was computed by differentiating the measured yaw-angle signal. The measured motion, rather than the commanded robotic-arm trajectory, was used throughout the aerodynamic derivative identification to ensure that the estimated derivatives corresponded to the actual kinematics experienced by the vehicle.

The yaw damping derivative was calculated as

$$N_r = \frac{\partial N}{\partial r}, \tag{1}$$

where $N$ is the yawing moment about the center of gravity and $r$ is the yaw rate. For each angle-of-attack and sideslip-

http://www.imavs.org/

angle condition, the variation of yawing moment with yaw rate was used to estimate $N_r$.

The side-force and roll-moment responses were also examined to assess whether other yaw-rate-related lateral–directional effects could be identified. However, the side-force response did not show a repeatable monotonic trend with increasing yaw rate, and the roll-moment curves were highly overlapped across yaw-sweep speeds. Therefore, the final quantitative identification in this paper focuses on $N_r$, while the $Y$ and $L$ responses are used qualitatively to interpret the limitations and dominant aerodynamic trends of the experiment.

## 3 Results and Discussion

### 3.1 *Lateral–directional force and moment response*

The processed experimental data show that the side force $Y$, yawing moment $N$, and rolling moment $L$ respond differently to sideslip angle and yaw-sweep speed. Each test condition was repeated five times. The solid curves in Figs. 4, 5, and 6 represent the mean response of the five runs, while the shaded regions denote $\pm 1$ standard deviation. The observed variability primarily reflects cycle-to-cycle variations in the unsteady flapping-wing aerodynamic loads and measurement uncertainty rather than poor repeatability of the robotic-arm motion.

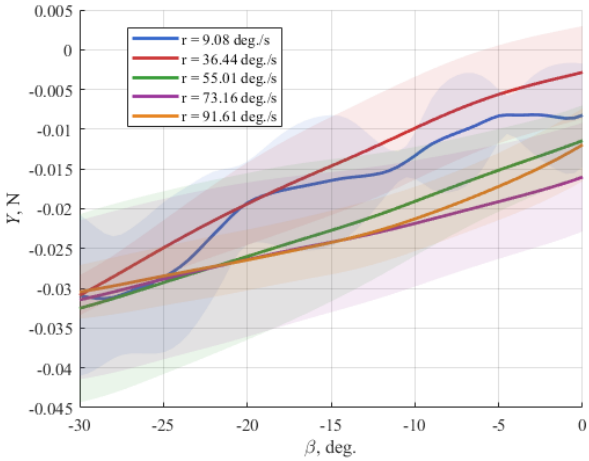


Figure 4: Mean side-force response as a function of sideslip angle at different yaw-sweep speeds for $\alpha = 60°$. Solid lines denote the mean of five repeated experiments, while the shaded regions indicate $\pm 1$ standard deviation. The response does not show a clear monotonic trend with increasing yaw rate.

Figure 4 shows the side-force response at $\alpha = 60°$. Although the side force varies with sideslip angle, the responses obtained at different yaw-sweep speeds do not exhibit a consistent monotonic dependence on yaw rate. The separation among the curves is comparable to the measurement variability, indicating that the yaw-rate contribution to side force is too small to permit reliable identification of the side-force derivative, $Y_r$.

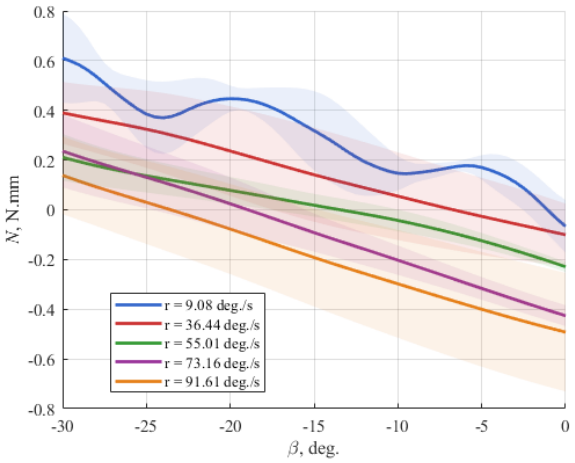


Figure 5: Mean yawing-moment response as a function of sideslip angle at different yaw-sweep speeds for $\alpha = 60°$. Solid lines denote the mean of five repeated experiments, while the shaded regions indicate $\pm 1$ standard deviation. The systematic separation among the curves demonstrates a measurable yaw-rate effect.

In contrast, the yawing-moment response shown in Fig. 5 exhibits a clear and repeatable dependence on yaw-sweep speed. As the yaw rate increases, the yawing-moment curves shift systematically, demonstrating that the yawing moment is sensitive to yaw-rate perturbations. This trend forms the basis for identifying the yaw damping derivative, $N_r$. Physically, the imposed yaw rate generates an additional lateral velocity at the tail, producing a restoring yawing moment. Consequently, the measured negative values of $N_r$ are consistent with the expected stabilizing directional damping of the tailed FWMAV.

Figure 6 shows that the rolling moment is governed primarily by sideslip angle. The roll moment increases approximately linearly as $\beta$ changes from $0°$ to $-30°$, while the responses at different yaw-sweep speeds remain highly overlapped. This indicates that the yaw-rate contribution to roll moment is small, suggesting that $L_r$ cannot be reliably identified under the present test conditions. Together with the side-force results, this demonstrates that the dominant measurable yaw-rate effect appears in the yawing moment.

### 3.2 *Identified yaw damping derivative*

The identified yaw-moment derivative with respect to yaw rate, $N_r$, remained negative across the tested conditions. This negative sign indicates that the yawing moment generated by the vehicle opposes the imposed yaw-rate perturbation. Therefore, the measured $N_r$ represents a stabilizing yaw-

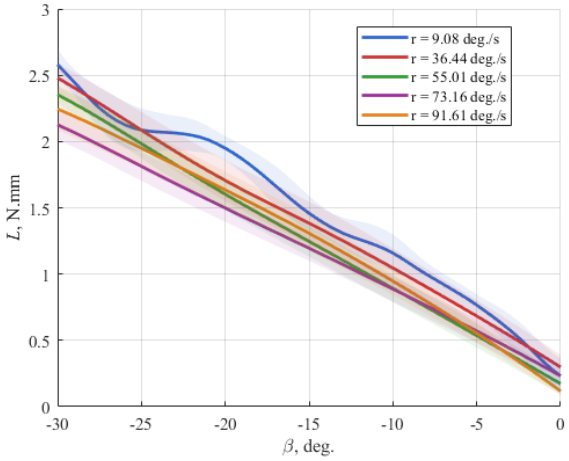


Figure 6: Mean rolling-moment response as a function of sideslip angle at different yaw-sweep speeds for $\alpha = 60°$. Solid lines denote the mean of five repeated experiments, while the shaded regions indicate $\pm 1$ standard deviation. The overlap among the curves suggests that the rolling moment is governed primarily by sideslip angle rather than yaw rate.

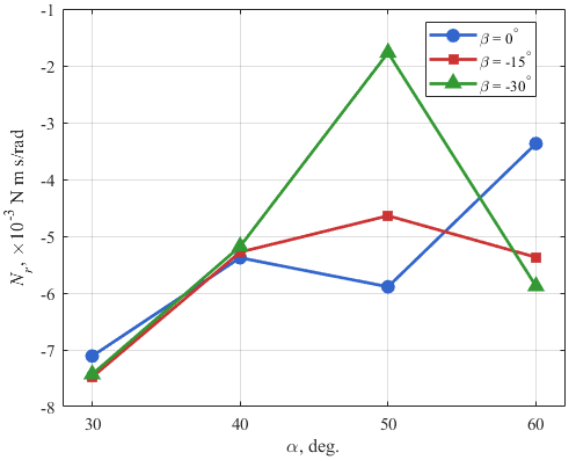


Figure 7: Identified yaw damping derivative, $N_r$, as a function of angle of attack for the three tested sideslip angles. The negative values indicate a stabilizing yawing moment opposing the imposed yaw-rate perturbation.

damping effect.

The magnitude of $N_r$ varied with angle of attack and sideslip angle, reflecting the influence of the high-angle flapping-wing flow field, tail interaction, and body orientation. Although the variation with angle of attack was not strictly monotonic, $N_r$ remained negative throughout the investigated flight envelope, indicating that the vehicle consistently generated a restoring yawing moment in response to yaw-rate perturbations.

Figure 7 summarizes the identified yaw damping derivative, $N_r$, as a function of angle of attack for the three tested sideslip angles. The measured $N_r$ values are generally on the order of $10^{-3}$ N m s/rad.

### *3.3 Comparison with DelFly II*

To assess the physical consistency of the identified yaw damping derivative, the result was compared with the dimensional yaw-rate derivative reported for DelFly II. Although the two platforms differ in geometry, wing configuration, tail arrangement, and test condition, DelFly II provides a useful reference because it is one of the few flapping-wing MAVs with reported lateral– directional aerodynamic derivatives.

Table 1 compares the dimensional yaw damping derivative obtained in this study with that reported for DelFly II. The comparison uses the present data at $\alpha = 60°$ because the DelFly II reference data were obtained at an approximately similar angle of attack. For example, using the reported velocity components $u = 0.25$ m/s and $w = 0.5$ m/s, the corresponding angle of attack is $\alpha = \tan^{-1}(w/u) \approx 63.4°$, which is close to the 60° condition tested in this study.

Table 1: Comparison of dimensional yaw damping derivative between DelFly II [9] and the present FWMAV.

| Derivative | DelFly II | Present study |
|---|---|---|
| $N_r$ (N m s/rad) | $-1.9 \times 10^{-3}$ | $-3.37 \times 10^{-3}$ |

The two values are of the same order of magnitude and have the same negative sign, indicating physically consistent yaw damping behavior. The difference in magnitude may be attributed to differences in vehicle geometry, flight speed, flapping amplitude, tail configuration, and aerodynamic scaling. The present experiment was conducted at a nominal incoming flow velocity of approximately 2 m/s, whereas the DelFly II aerodynamic model was identified from near-hover and slow-forward-flight maneuvers at approximately 0.5 m/s [9]. Nevertheless, the negative $N_r$ value observed in both platforms indicates that yaw-rate perturbations generate a restoring yawing moment, which is consistent with stable lateral–directional damping behavior. Although obtained using different experimental methodologies, the agreement in both sign and order of magnitude provides additional confidence that the identified yaw damping derivative is physically reasonable.

## 4 Conclusion

This paper presented an experimental method for identifying yaw damping in a tailed flapping-wing micro air vehicle. A synchronized robotic-arm-based test platform was used to impose controlled yaw motions under prescribed angle-of-attack and sideslip conditions. The measured force, moment, attitude, and yaw-rate data were processed to evaluate the lateral–directional aerodynamic response to yaw-rate

http://www.imavs.org/

perturbations.

The results show that the yawing moment exhibits a clear and repeatable dependence on yaw rate, allowing the yaw damping derivative $N_r$ to be identified. The identified $N_r$ remained negative across the tested conditions, indicating that the vehicle generates a yawing moment opposing yaw-rate perturbations. This confirms the presence of stable yaw damping for the present FWMAV configuration.

The side-force response did not show a clear repeatable trend with increasing yaw rate. This suggests that the yaw-rate effect on side force is too small to be reliably captured by the present experimental setup. The roll-moment response showed a strong dependence on sideslip angle but only weak dependence on yaw-sweep speed, indicating that the roll moment is primarily sideslip-dominated rather than yaw-rate-dominated.

These findings provide experimental evidence of yaw damping in a tailed FWMAV and support future lateral–directional dynamic modeling and flight control design. Future work will improve the measurement sensitivity, further characterize the fan-array inflow, extend the experimental envelope, include rudder-input excitation, and incorporate the identified yaw damping derivative into a complete lateral–directional state-space model. In addition, the proposed identification protocol will be evaluated using reference models or simulated datasets with known aerodynamic derivatives to further assess the accuracy and robustness of the estimation method.


## ACKNOWLEDGEMENTS

This work was supported by the National Science and Technology Council, Taiwan, under Grant NSTC 114-2221-E-006-063.


## REFERENCES


[1] M. H. Dickinson, F. O. Lehmann, and S. P. Sane. Wing rotation and the aerodynamic basis of insect flight. *Science*, 284:1954–1960, 1999.

[2] S. P. Sane. The aerodynamics of insect flight. *Journal of Experimental Biology*, 206(23):4191–4208, 2003.

[3] W. Shyy, M. Berg, and D. Ljungqvist. Flapping and flexible wings for biological and micro air vehicles. *Progress in Aerospace Sciences*, 35:455–505, 1999.

[4] J. M. Birch and M. H. Dickinson. Spanwise flow and the attachment of the leading-edge vortex on insect wings. *Nature*, 412:729–733, 2001.

[5] H. E. Taha, M. R. Hajj, and A. H. Nayfeh. Flight dynamics and control of flapping wing mavs: A review. *Nonlinear Dynamics*, 70:907–939, 2012.

[6] Q. Khan and R. Akmeliawati. Review on system identification and mathematical modeling of flapping-wing micro aerial vehicles. *Applied Sciences*, 11:1546, 2021.

[7] K. Nguyen, L. T. K. Au, H.-V. Phan, and H. C. Park. Comparative dynamic flight stability of insect-inspired flapping-wing micro air vehicles in hover: Longitudinal and lateral motions. *Aerospace Science and Technology*, 119:107085, 2021.

[8] M. Y. Bhatti, S.-G. Lee, and J.-H. Han. Dynamic stability and flight control of biomimetic flapping-wing micro air vehicle. *Aerospace*, 8:362, 2021.

[9] J. V. Caetano, C. C. de Visser, G. C. H. E. de Croon, B. Remes, C. de Wagter, J. Verboom, and M. Mulder. Linear aerodynamic model identification of a flapping wing mav based on flight test data. *International Journal of Micro Air Vehicles*, 5(4):273–286, 2013.

[10] S. F. Armanini, M. Karásek, and C. C. de Visser. Global linear parameter-varying modeling of flapping-wing dynamics using flight data. *Journal of Guidance, Control, and Dynamics*, 41:2338–2360, 2018.

[11] D. D. Vicroy. A guide to forced oscillation data processing and analysis. Technical Report NASA/TP–20210023569, NASA, 2023.

[12] W.-L. Chan, D.-J. Liu, H.-Y. Chen, and C.-L. Chin. A fan-array robotic-arm approach to characterization of pitch-rate dynamics of a flapping-wing mav. *Actuators*, 14(12):592, 2025.

[13] B. Cheng and X. Deng. Translational and rotational damping of flapping flight and its dynamics and stability at hovering. *IEEE Transactions on Robotics*, 27(5):849–864, 2011.

[14] L. Ristroph, G. Ristroph, S. Morozova, A. J. Bergou, S. Chang, J. Guckenheimer, Z. J. Wang, and I. Cohen. Active and passive stabilization of body pitch in insect flight. *Journal of The Royal Society Interface*, 10(85):20130237, 2013.


http://www.imavs.org/